Advances in Applied Sciences
2026, Vol. 11, No. 2, pp. 30–43
https://doi.org/10.11648/j.aas.20261102.12

Research Article

Study of the Equilibrium Composition of an Air Plasma Contaminated by H_2S, Cl_2, and SO_2

Yaguibou Wepari Charles[1, *], Beogo Cedric[1], Korbeogo Aly Rachid[2], Pafadnam Ibrahim[3], Banouga Adjigkiga[3], Koalaga Zacharie[4]

[1]Country Dori University Center, Thomas Sankara University, Ouagadougou, Burkina Faso

[2]Department of Mathematics, Physics and Engineering Sciences, Preparatory Classes for Engineering Studies (CPEI) Polytechnic School of Ouagadougou, Ouagadougou, Burkina Faso

[3]Department of Physics, Training and Research Unit in Science and Technology, Thomas Sankara University, Ouagadougou, Burkina Faso

[4]Department of Physics, Training and Research Unit in Exact and Applied Sciences, Joseph Ki-Zerbo University, Ouagadougou, Burkina Faso

Abstract

Dust and corrosive atmospheres severely impact the dielectric strength of the switching chamber and moving parts in air circuit breakers. Within the arc-quenching chamber, the switching medium must possess sufficient deionization capability to ensure its dielectric recovery. However, this capability can be significantly compromised by the presence of corrosive species such as H_2S, Cl_2, and SO_2. These impurities can lead to an increase in contact resistance through contact corrosion, as well as the generation of leakage currents. Thus, the objective of this study is to highlight the impact of H_2S, Cl_2, and SO_2 species on the equilibrium composition of air plasma at atmospheric pressure and under local thermodynamic equilibrium (LTE) conditions. The Gibbs free energy minimization method is used to determine the plasma equilibrium composition. The results reveal a complete modification of the plasma equilibrium composition due to the presence of these impurities, characterized by the formation of species such as Cl_2, S_2, NOCl, HCl, HOCl, H_2, SH, S_2O, HO_2, ClO, SO_3, SO_2, NO, SO, SCl and SN, whose concentrations vary depending on the impurity percentage. It is shown that the presence of HCl and Cl_2 accelerates contact corrosion. Furthermore, a significant increase in electron density is observed between 5,000 K and 14,000 K. This phenomenon induces a rise in electrical conductivity, which could ultimately lead to a current interruption failure.

Keywords

Air Circuit Breaker, Arc-quenching Medium, Chemical Equilibrium, Gibbs Free Energy Minimization, Electron Density, Corrosive Impurities

*Correspondence: Yaguibou Wepari Charles (weparicharles@gmail.com)

Received: 30 May 2026; **Accepted:** 27 June 2026; **Published:** 22 July 2026

1. Introduction

The circuit breaker is one of the essential components for the safety of electrical networks, ensuring the protection of equipment through the controlled interruption of fault currents. The efficiency of an air circuit breaker relies on its capacity to transform an initially insulating medium (air) into a conducting medium via the creation of an electric arc, and subsequently to dissipate the energy of this plasma to restore dielectric insulation within a few milliseconds [1].

However, this current interruption process is inherently sensitive to environmental conditions. Indeed, air circuit breakers are open systems exposed to the external environment [2]. They are frequently deployed in harsh environments, facing adverse conditions such as humidity, heat, dust, and corrosive atmospheres. Such exposure, particularly to dust and corrosive gases, significantly impacts their performance and operational lifespan [3]. For instance, high ambient temperatures promote the ageing of plastic insulators, which degrades the mechanical properties of components and causes the hardening of grease, thereby hindering the operation of the device. Humidity leads to metal corrosion, promoting the formation of rust on iron, zinc, copper, and silver. This results in increased friction and risks of mechanical failure, consequently elevating contact resistance and reducing insulation. Furthermore, the deposition of dust and corrosive species such as sulphur dioxide, chlorine, ammonia, and nitrogen oxides induces oxidation reactions. These reactions can cause mechanical jamming, excessive overheating, short-circuiting, and an increase in contact resistance [3]. Consequently, this polluted environment profoundly alters the thermodynamic properties and transport coefficients of the gaseous medium.

Previous research has extensively investigated electric arc interruption in various media. For example, Yaguibou et al. studied the influence of aerosols on circuit breaker performance and concluded that aerosols adversely affect the operation of air circuit breakers by degrading the thermophysical properties of the plasma [4-8]. This can lead to interruption failure, the formation of oxide layers within the arc chamber, and post-interruption leakage currents [5, 6]. Similarly, Cressault et al., and Banouga et al. demonstrated that metallic vapours within the plasma increase electrical conductivity while decreasing specific enthalpy and thermal conductivity [9-14]. Conversely, Kagone et al., and Kohio et al. showed that water vapour can improve arc interruption performance by increasing the thermal conductivity of the plasma, thereby reducing the arc-quenching duration [15-20].

Furthermore, recent developments in switching media reflect a sustained research effort to understand the physicochemical interactions within the arc plasma. Alternatives to SF_6, such as C_4F_7N/CO_2, mixtures, exhibit reduced arc temperatures and diffusion distances compared to pure SF_6 [21], while maintaining comparable interruption performance and drastically lowering the global warming potential [22]. However, their dielectric properties are highly dependent on synergistic effects among the gas mixture constituents [23]. In addition, metallic vapor from contact erosion significantly alters their chemical decomposition pathways under high-temperature arcs [24]. Consequently, contact erosion remains a decisive factor in the progressive degradation of the circuit breakers' breaking capacity [25].

Although Charles et al. recently investigated the impact of chlorine (Cl_2) and hydrogen sulphide (H_2S) on the thermophysical properties of air plasma [26], no study has yet examined, to our knowledge, the simultaneous impact of chlorine (Cl_2), sulphur dioxide (SO_2), and hydrogen sulphide (H_2S) on the equilibrium composition and thermophysical properties of air plasma in low-voltage circuit breakers.

The primary objective of this work is therefore to analyse the joint influence of Cl_2, SO_2, and H_2S on the equilibrium composition of air plasma in a low-voltage air circuit breaker during the current interruption phase. This study is conducted at atmospheric pressure and under local thermodynamic equilibrium (LTE), across a temperature range spanning from 1,000 K to 30,000 K.

The remainder of this paper is structured as follows: the first section describes the Gibbs free energy minimisation method applied to determine the plasma equilibrium composition under LTE. The second section presents and discusses the calculation results. Finally, the third section provides the conclusion and outlines future prospects.

2. Materials and Methods

The composition of the electric arc plasma is determined using the Gibbs free energy minimisation method under the assumption of local thermodynamic equilibrium (LTE). The minimisation of the Gibbs free energy and the resolution of the coupled Saha-Boltzmann and Guldberg-Waage equations are strictly equivalent under LTE [27]. The primary advantage of the Gibbs free energy minimisation method is that it avoids the arbitrary selection of a set of independent chemical reactions. Under LTE, the plasma is characterised by a single local temperature where collisional processes dominate, thereby enabling the application of the Maxwell-Boltzmann distribution and the Saha equation to determine the species concentrations [28, 29].

A total of 100 chemical species are considered in our calculations, assuming that all constituents are in the gaseous state:

Electron: e^-

23 monoatomic species (atoms and ions): S, O, N, H, Cl, H^+, H^-, O^-, O^+, N^+, N^-, Cl^-, Cl^+, S^+, S^-, O^{++}, N^{++}, S^{++}, Cl^{++}, O^{+++}, N^{+++}, S^{+++}, Cl^{+++}.

27 diatomic species: H_2, O_2, N_2, S_2, Cl_2, HCl, OH, NO, NH, SH, SO, SCl, SN, ClO, H_2^+, H_2^-, O_2^+, O_2^-, OH^+, OH^-, NO^+, N_2^+, N_2^-, NH^+, SH^-, SO^-, S_2^-.

49 polyatomic species: HNO, H_2O, HNO_2, HO_2, HNO_3,

H_2O_2, H_2S, H_2SO_4, HOCl, O_3, N_3, NO_2, N_2O, NH_2, N_3H, N_2H_2, NH_3, N_2H_4, NO_3, NOCl, NO_2Cl, N_2O_3, N_2O_4, N_2O_5, NH_2OH, NH_2NO_2, SO_2, SCl_2, SO_2Cl_2, SO_3, S_2Cl_2, S_2O, S_3, S_4, S_5, S_6, S_7, S_8, ClO_2, Cl_2O, HO_2^-, H_2O^+, H_3O^+, N_2O^+, NH_4^+, NO_3^-, NO_2^-, SCl_2^+, SO_2^-.

Evaluating the equilibrium composition requires knowledge of the specific chemical potentials of each particle [28-30]. For electrons and heavy species (atoms and molecules), these potentials are calculated using specific enthalpies and entropies obtained from the National Institute of Standards and Technology (NIST), Bonnie, and Bendjebbar databases [30-32]. In this study, Bonnie's smoothed data are preferred to express the thermodynamic properties as a function of temperature [30, 32]:

$$\begin{cases} C_{P_i}^0 = a_1T^{-2} + a_2T^{-1} + a_3 + a_4T + a_5T^2 + a_6T^3 + a_7T^4 \\ \frac{H_i^0}{RT} = -a_1T^{-2} + a_2\frac{ln(T)}{T} + a_3 + a_4\frac{T}{2} + a_5\frac{T^2}{3} + a_6\frac{T^3}{4} + a_7\frac{T^4}{5} + \frac{b_1}{T} \\ \frac{S_i^0}{R} = -a_1\frac{T^{-2}}{2} + a_2\frac{T^{-1}}{2} + a_3ln(T) + a_4T + a_5\frac{T^2}{2} + a_6\frac{T^3}{3} + a_7\frac{T^4}{4} + b_2 \end{cases} \quad (1)$$

where R is the ideal gas constant and T is the temperature in kelvins. The coefficients a_i and b_i for each particle are extracted from Bonnie's data [30, 32].

The specific chemical potential of a species i is obtained from its specific enthalpy and specific entropy as follows [32, 33]:

$$\mu_i^0 = H_i^0 - TS_i^0 + \Delta H_{fi}^0 \quad (2)$$

where ΔH_{fi}^0 represents the standard enthalpy of formation of species *i*.

To determine the concentrations of the various chemical species, the Gibbs free energy minimisation method is employed [8, 13, 28-35]. The chemical species concentrations (denoted as y_i) must satisfy electrical quasi-neutrality and the conservation of nuclei (element conservation) within the plasma [32, 34]. These two conditions are expressed as the following constraints:

$$\sum_{i=1}^{N} a_{ij}y_i = b_j(j = 1, 2, \dots m) \quad (3)$$

where N is the number of chemical species in the mixture, m represents the number of constraints (five chemical elements plus the electron), a_{ij} is the number of nuclei of type *j* contained in chemical species *i*, and b_j represents the initial number of nuclei of type *j*. In our plasmas, six different types of nuclei are considered: e^-, H, O, N, S, and Cl.

The Gibbs free energy evaluated at point Y (y_1, y_2, y_N,) yields:

$$G(Y) = \sum_{i=1}^{N} y_i\left(C_i + RT\ln\left(\frac{y_i}{\sum_{k=1}^{N} y_k}\right)\right) \quad (4)$$

with

$$C_i = \mu_i^0 + RT\ln\left(\frac{P}{P_0}\right) \quad (5)$$

The y_i values are proportional to the number densities n_i. We seek the point that minimises the function G (Y), where the coordinates satisfy the following conditions:

1) The concentrations n_i must be positive, hence $y_i \geq 0\ \forall\ i$
2) The coordinates y_i must satisfy the conservation of the number of nuclei and electrical neutrality.

A second-order Taylor series expansion around point $Y(y_1, y_2, y_3, \dots, y_M)$ yields:

$$Q(X) = \mathrm{G(Y)} + \sum_{i=1}^{N}\left(\frac{\partial G}{\partial x_i}\right)_{X=Y}(x_i - y_i) + \frac{1}{2}\sum_{i=1}^{N}\sum_{k=1}^{N}\left(\frac{\partial^2 G}{\partial x_i \partial x_k}\right)_{X=Y}(x_i - y_i)(x_k - y_k) \quad (6)$$

To consider the physical conditions (3), the Lagrange multipliers π_j are introduced. This yields the new function $\zeta(X)$:

$$\zeta(X) = Q(X) + \sum_j \pi_j(-\sum a_{ij}x_i + b_j) \quad (7)$$

Let us determine the minimum of $G(X)$ using relation [33, 35] $\frac{\partial\varsigma(X)}{\partial x_i} = 0$.

$$\frac{\partial\zeta(X)}{\partial x_i} = \sum_i^N(x_i - y_i)\left(C_i + RT\ln\left(\frac{y_i}{\sum_k^N y_k}\right)\right) + \frac{1}{2}\sum_i^N RT\left(\frac{x_i - y_i}{y_i} - \frac{\sum_{k=1}^{N}(x_k - y_k)}{\sum_k^N y_k}\right) + \sum_j^m \pi_j a_{ij} \quad (8)$$

Which leads to:

$$\frac{f_i}{y_i} = RT\left(\frac{x_i - y_i}{y_i} - \frac{\sum_{k=1}^{N}(x_k - y_k)}{\sum_k^N y_k}\right) - \sum_{j=1}^{m}\pi_j a_{ij} = 0 \quad (9)$$

with

$$f_i = y_i\left(C_i + RT\ln\left(\frac{y_i}{\sum_{k=1}^{N} y_k}\right)\right) \quad (10)$$

Using the Newton-Raphson method, the following system of equations is obtained [32, 34, 36]:

$$\begin{pmatrix} \frac{RT}{y_1} & \cdots & 0 & a_{11} & \cdots & a_{1m} \\ \vdots & \ddots & \vdots & \vdots & \ddots & \vdots \\ 0 & \cdots & \frac{RT}{y_N} & a_{N1} & \cdots & a_{Nm} \\ a_{11} & \cdots & a_{N1} & 0 & \cdots & 0 \\ \vdots & \ddots & \vdots & \vdots & \ddots & \vdots \\ a_{1m} & \cdots & a_{Nm} & 0 & \cdots & 0 \end{pmatrix} \begin{pmatrix} \Delta x_1 \\ \vdots \\ \Delta x_N \\ \Delta \pi_1 \\ \vdots \\ \Delta \pi_m \end{pmatrix} = \begin{pmatrix} -\mu_1 - \mathrm{RT}ln\left(\frac{y_1}{\sum_i^N y_i}\right) - \mathrm{RT}ln\left(\frac{P}{P_0}\right) - \sum_{j=1}^m \pi_j a_{ij} \\ \vdots \\ -\mu_N - \mathrm{RT}ln\left(\frac{y_N}{\sum_i^N y_i}\right) - \mathrm{RT}ln\left(\frac{P}{P_0}\right) - \sum_{j=1}^m \pi_j a_{ij} \\ -\sum_{i=1}^N y_i a_{i1} + b_1 \\ \vdots \\ -\sum_{i=1}^N y_i a_{im} + b_m \end{pmatrix} \quad (11)$$

with $x_i = y_i$.

In this study, one hundred (100) chemical species were considered, thus, N = 100. Consequently, the system of equations (11) consists of one hundred and six (106) equations with one hundred and six (106) unknowns, which are the number of moles of the one hundred (100) chemical species plus the six (6) Lagrange multipliers.

To solve equation (11), initial values are arbitrarily assigned to the number of moles y_i (where $\epsilon\,[1, 100]$) and to the Lagrange multipliers π_i (where $i\,\epsilon\,[1, 6]$). These initial mole numbers must satisfy condition (3), namely:

$$\begin{cases} y_i \geq 0 \\ \sum_i^N a_{ij} y_i = b_j \end{cases} \quad j = 1, \ldots, 6 \quad (12)$$

System of equations (11) is solved, and the new values of the mole numbers and Lagrange multipliers are obtained using the following relation:

$$\begin{cases} x_i = y_i + \lambda \Delta x_i & \forall\, i \in [1, N] \\ \pi_j = \pi_j + \lambda \Delta \pi_j & \forall\, j \in [1, m] \end{cases} \quad (13)$$

The correction parameter λ is the largest value between 0 and 1. It must satisfy the following condition:

$$x_i = y_i + \lambda \Delta x_i > 0 \quad \forall\, i \in [1, N] \quad (14)$$

This step prevents negative mole numbers that may arise when moving away from the solution. The new values of the mole numbers and Lagrange multipliers are then used for a new calculation cycle. The convergence criterion to terminate the iterations is determined by the following condition [34]:

$$\frac{(G(X) - G(Y))}{G(X)} < 10^{-14} \quad \forall\, i \in [1, N] \quad (15)$$

The number densities are obtained using the following Dalton's law [11]:

$$n_i = x_i \frac{\frac{P - \Delta P}{k}}{\sum_{i=1}^N T_i x_i} \quad (16)$$

Where $\Delta P = -\frac{1}{24}\frac{kT}{\pi \lambda_D^3}$ the lowering of the pressure, and $\lambda_D = \sqrt{\frac{\varepsilon_0 kT}{e^2 \sum_{i=1}^N n_i Z_i^2}}$ the Debye length.

3. Results

3.1. Validation of the Calculation Method

To validate our calculation program developed using MATLAB software, a comparison of the air plasma composition at local thermodynamic equilibrium (LTE) and atmospheric pressure was performed against data from Powars *et al.,* and Bacri *et al.* The data are compiled in Table 1 [37, 38]. The temperatures considered are 2000 K and 15,000 K. At 2000 K, an excellent agreement is observed between our results and those of Powars *et al.* At this temperature, the majority species are nitrogen (N_2) and oxygen (O_2). Discrepancies of 2.01% for nitrogen and 7.14% for oxygen are observed. A maximum discrepancy of 3% is also noted with the data from Bacri *et al.* A divergence is observed at 2000 K for monoatomic species. This divergence could be attributed to the thermodynamic data used and the calculation method chosen for the equilibrium composition. At 15,000 K, the mixture is highly ionised. Electrons, as well as N^+ and O^+ ions, become the majority species. The discrepancy between our data and those of Powars *et al.,* and Bacri *et al.,* does not exceed 7% for monoatomic species. Nitrogen and oxygen molecules exhibit discrepancies of around 21%. However, they are minority species at 15,000 K. Thus, the majority species show a discrepancy of less than 10% compared to the literature. The largest discrepancies are observed for minority species, thereby confirming the consistency of our results with the literature.

Table 1. Comparison of chemical species mole fractions in the air plasma.

Particules	Powars et al.	Bacri et al.	results	Gap with Powars et al. [37]	Gap with Bracri et al. [38]	Powars et al.	Bacri et al.	results	Gap with Powars et al. [37]	Gap with Bacri et al. [38]
2000 K						15000 K				
e^-	-	-	-	-	-	3.46E-1	3.43E-1	3.41E-1	1.47	0.60
O	3.00E-4	3.94E-4	2.96 E-4	1.35	33.10	8.01E-2	7.99E-2	7.78E-2	2.95	2.70
N	8.40E-10	1.18E-9	8.04E-10	4.48	46.76	2.25E-1	2.31E-1	2.39E-1	5.86	3.34
O_2	2.10E-1	2.02E-1	1.96E-1	7.14	3.06	-	3.22E-8	2.80E-08	-	15.26
N_2	7.80E-1	7.73E-1	7.96E-1	2.01	2.89	3.55E-6	3.25E-6	4.12E-06	13.83	21.11
O^+	-	-	-	-	-	5.74E-2	5.77E-2	5.40E-2	6.29	6.85
N^+	-	-	-	-	-	2.87E-1	2.817E-1	2.75E-1	4.36	2.18

3.2. Calculation of Dry Air Plasma Equilibrium Composition

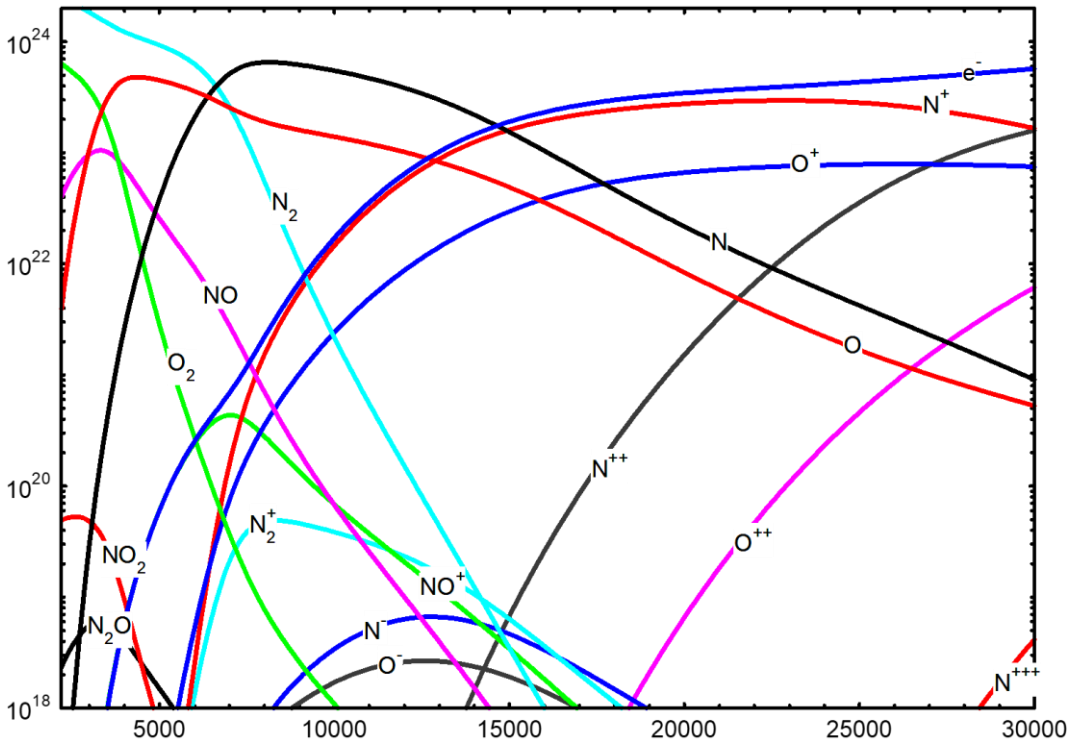

Figure 1. Equilibrium composition of dry air plasma as a function of temperature.

Figure 1 shows the evolution of the dry air equilibrium composition as a function of temperature. This profile is divided into three distinct zones. The first zone corresponds to temperatures below 5000 K. Within this temperature range, N_2, O_2, and NO are the majority species in the plasma. The NO_2 and N_2O molecules are minority species and completely dissociate below 5000 K. The density of NO^+ ions increases with temperature, and electroneutrality is rigorously established between electrons and these NO^+ ions. For temperatures ranging from 5000 K to 15,000 K, the atomic species N and O become predominant, while the concentrations of N^+ and O^+ ions, along with electrons progressively increase. Conversely, the N and O species subsequently decrease with temperature. The N_2 fraction drops rapidly, whereas O_2 and NO disappear before 15,000 K. The disappearance of these molecules via dissociation is precisely what causes the increase in neutral atoms. Furthermore, the NO^+ ion reaches its peak around 7000 K before decreasing rapidly. The N_2^+, N^-, and O^- ions remain

minority species. Nonetheless, the presence of the negative ions N^-, and O^- influences the electrical conductivity, as they capture electrons and thus reduce their number density. As for temperatures above 15,000 K, the plasma is predominantly ionised. Electrons, as well N^+ and O^+ ions become the majority species. An increase in doubly ionised N^{++} and O^{++} ions is also observed. In this region, electroneutrality is essentially maintained between electrons and the N^+ and O^+ ions.

3.3. Impact of Pollutants on Air Composition

Figures 2 to 5 present the evolution of the equilibrium composition of the plasma contaminated by Cl_2, H_2S, and SO_2 pollutants.

For temperatures below 5000 K, the medium is dominated by neutral species, with N_2 and O_2 being the majority components. The presence of H_2S, Cl_2, and SO_2 gives rise to species such as NOCl, HCl, Cl_2, HOCl, H_2, SH, S_2O, HO_2, ClO, SO_3, SO_2, NO, SO, SCl, and SN. High number densities of HCl, Cl_2, de SO_3, and SO_2 are observed at temperatures below 3000 K. SO_3 decreases rapidly and disappears at approximately 4000 K, whilst SO_2 dissociates circa 4000 K. Cl_2 undergoes dissociation between 1500 K and 2000 K. H_2 reaches its peak density around 3500 K. The high concentration of HCl is likely linked to the reaction between Cl_2 and H. ClO dissociates at approximately 3000 K, whereas SO, SH, and SCl dissociate around 3700 K. The species OH, S_2, and SN dissociate at approximately 3200 K, 4000 K, and 4500 K, respectively. These various molecular dissociation reactions lead to the appearance and subsequent density increase of atomic species such as Cl, S, N, O. and H. Furthermore, the species NO_2, N_2O, HOCl, HO_2, H_2, SH, S_2O, and NOCl remain minority components. The densities of NO^+ ions and electrons increase with temperature. The onset of Cl^- ions is also observed around 3000 K. although this species remains highly minor. Electroneutrality is strictly established between electrons and NO^+ ions.

In the temperature range between 5000 K and 15000 K. the plasma becomes progressively dominated by atoms and ions. The predominant species are N and O, followed by S, H, and Cl. All polyatomic species are fully dissociated below 5000 K. The concentrations of O_2, SO_2, N_2, NO, and SN decrease with increasing temperature. Specifically, SO_2, S_2, SH, and SCl vanish before 8000 K. Concurrently, Cl^+, S^+, O^+, and N^+ ions increase with temperature. NO^+ and N_2^+ reach their respective maxima around 7000 K and 10,000 K. The appearance of these ionic species strictly follows the hierarchy of ionization potentials: NO (9.264 eV), S (10.360 eV), Cl (12.968 eV), H (13.598 eV), O (13.618 eV), and N (14.534 eV) [31]. This hierarchy is not solely characteristic of the plasma phase. Indeed, on the electrode side, the electronic structure of the contact materials also governs both their wettability by the liquid pool and their arc resistance [39]. In addition to Cl^-, the presence of O^- and N^- is noteworthy. These negative ions serve to capture electrons, thereby reducing the electrical conductivity of the plasma, which greatly facilitates arc extinction. Electroneutrality is maintained between electrons and both S^+, and NO^+ ions up to 7000 K, and subsequently between electrons and S^+, O^+, and N^+ ions.

For temperatures exceeding 15,000 K. the plasma is virtually fully ionized, being dominated by O^+ and N^+ ions. S^+, Cl^+, and H^+ ions also account for significant fractions. Atomic N and O are still present but are no longer the majority species. Additionally, the emergence of multiply charged ions namely O^{2+}, N^{2+}, S^{2+}, Cl^{2+}, Cl^{3+}, N^{3+}, and S^{3+} is observed as temperature rises. The densities of S^{2+}, Cl^{2+}, Cl^{3+}, N^{3+}, and S^{3+} are strongly dependent upon the proportions of impurities within the mixture. Moreover, S^{2+} and Cl^{2+} appear earlier than O^{2+} and N^{2+}. This behaviour is attributed to the lower ionization energies of S and Cl compared to those of O and N. Finally. electroneutrality is established between electrons and N^+ and O^+ ions.

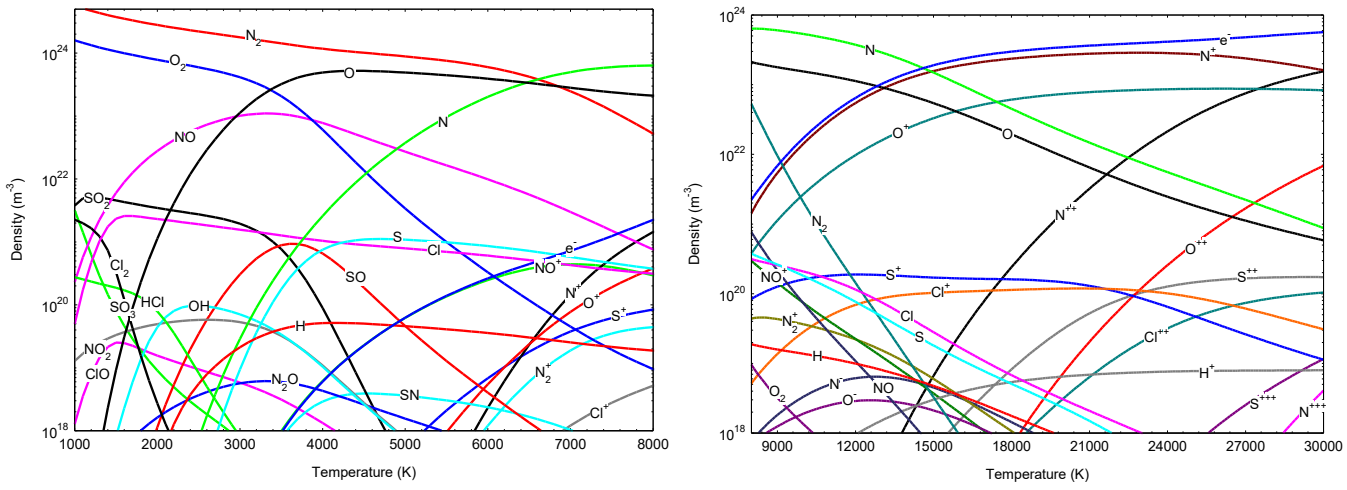

(a) (b)

Figure 2. *Equilibrium composition of a 99.9% pure air plasma (a, and b).*

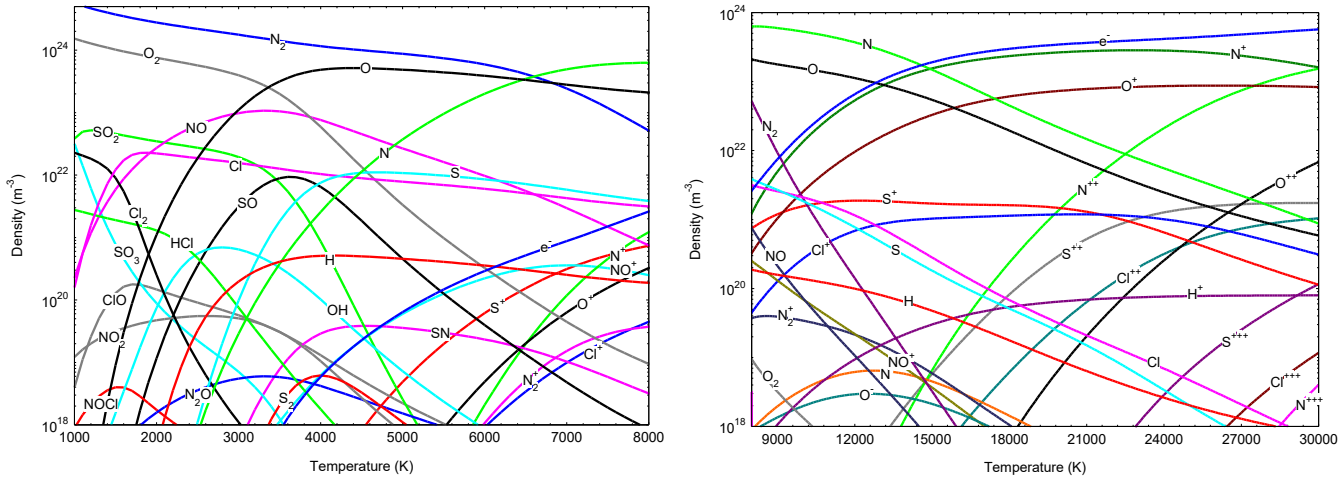

(a) (b)

Figure 3. *Equilibrium composition of a 99% pure air plasma (a, and b).*

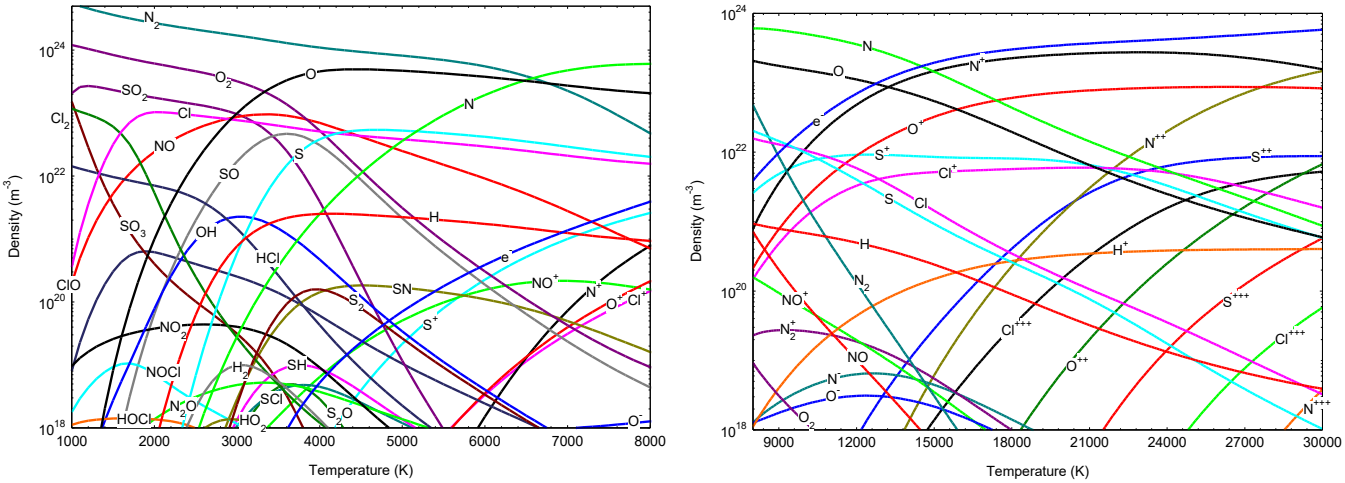

(a) (b)

Figure 4. *Equilibrium composition of a 95% pure air plasma (a, and b).*

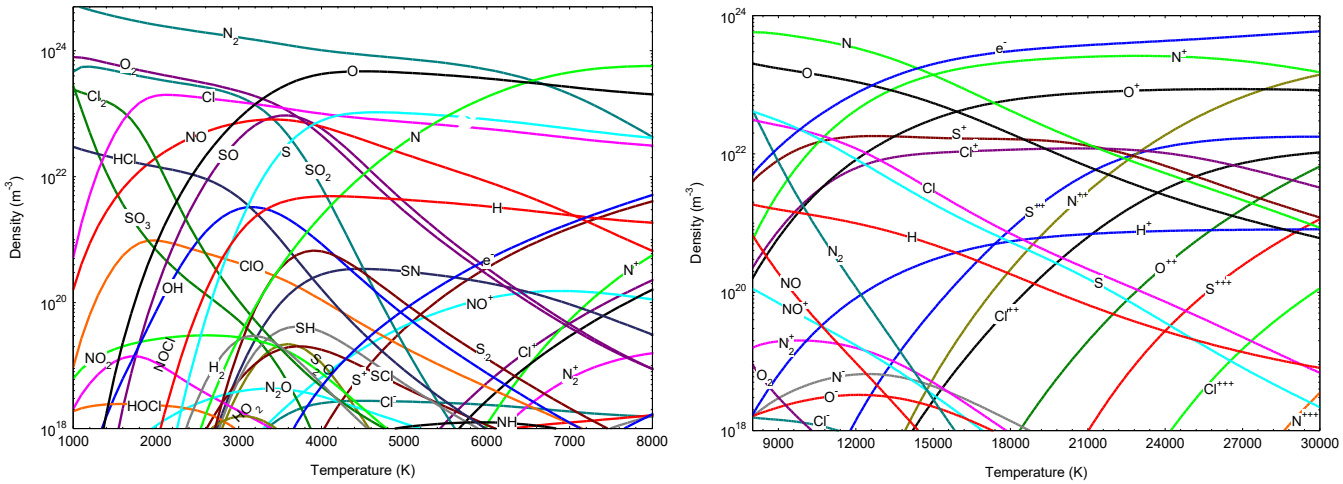

(a) (b)

Figure 5. *Equilibrium composition of a 90% pure air plasma (a, and b).*

Figure 6 illustrates the evolution of the electron density as a function of the percentage of impurities within the plasma. Generally, the curves exhibit the same trend. increasing monotonically with temperature. For temperatures below 5000 K, the addition of H_2S, SO_2, and Cl_2 contributes to a decrease in electron density as their percentage increases. This can be attributed to the rising concentration of molecular species such as Cl_2, S_2, NOCl, HCl, Cl_2, HOCl, H_2, SH, S_2O, HO_2, ClO, SO_3, SO_2, NO, SO, SCl, and SN. Indeed, these species undergo dissociation at low temperatures, thereby absorbing the energy available in the medium. This energy consumption subsequently delays electron production. Furthermore, the increased density of negative ions, such as Cl^-, considerably affects the electron density. Between 5000 K and 14,000 K, the electron density increases with the impurity content. This trend is justified by the complete dissociation of molecules into atoms. Certain atomic species, such as Cl and S, possess low ionization energies, thus, contributing to the enhancement of the electron density. In contrast, O, N, and H exhibit higher ionization energies (S: 10.36 eV, Cl: 12.97 eV, H: 13.60 eV, O: 13.62 eV, and N: 14.53 eV) [31]. Beyond 14000 K. the curves virtually overlap as the plasma becomes almost fully ionized.

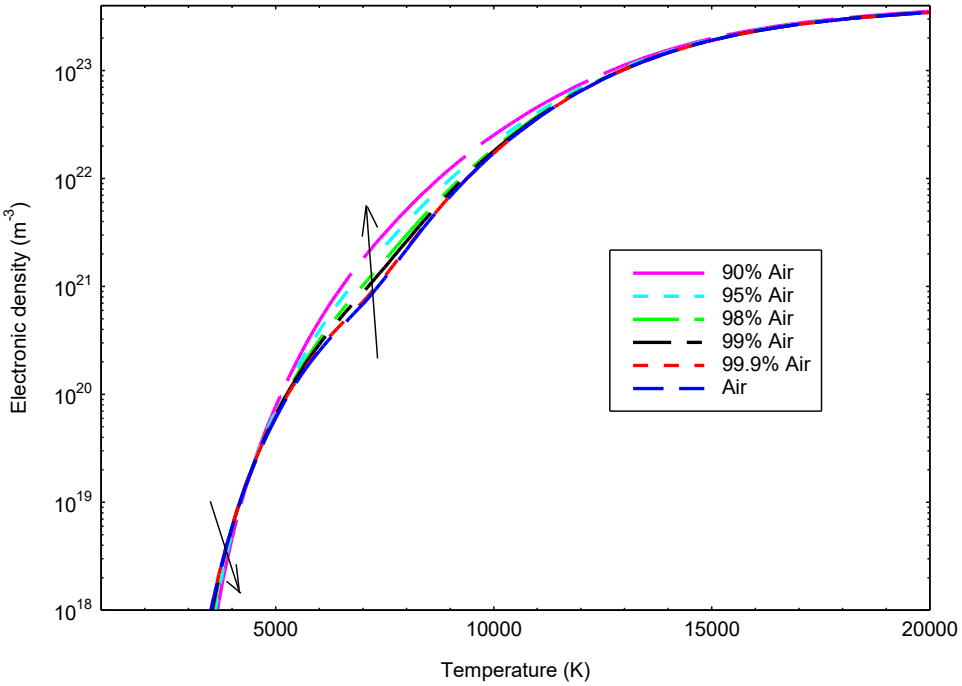

Figure 6. *Evolution of the plasma electron density as a function of the impurity percentage.*

4. Discussion

The critical thermal boundary for arc interruption in low-voltage circuit breakers was experimentally established by Christian *et al.,* at approximately 4200 K [40]. This represents the temperature measured within the contact zone just prior to the occurrence of a reignition, corresponding to a critical residual current density of the order of 5 A/cm^2. Fréton et al., confirmed that reignitions generally occur in regions where the gas temperature exceeds 4000 K [41]. The upper bound of this critical thermal window, situated between 7000 K and 8000 K is determined from the transport properties of the air plasma. Boulos et al., as well as Trelles *et al.*, demonstrated that the electrical conductivity of plasma gases exhibits a critical temperature (7000 K), below which it tends towards zero and above which it increases rapidly [42, 43]. Below 4000-5000 K, deionization is therefore sufficient to ensure dielectric recovery, as the electrical conductivity of the air becomes inadequate to sustain the arc [40-43]. Conversely, above 7000-8000 K, the electrical conductivity is high enough to maintain the arc because deionization remains incomplete, and the residual charge carriers compromise dielectric recovery [42-44].

Within this context, the presence of reactive species such as sulphur and chlorine inside the plasma significantly alters its transport properties. The early ionisation of sulphur and chlorine, whose ionisation potentials are lower than those of atomic nitrogen and oxygen, could lead to an increase in electron density and, consequently, in the electrical conductivity of the plasma [45, 46]. Furthermore, the dissociation peaks of SO_2, SO, HCl, and SCl contribute to the reactive thermal conductivity, thereby promoting radial energy transfer and the cooling of the arc channel [45, 46]. However, the formation of HCl and SO_2 at the cold periphery of the plasma poses a risk

to both the electrodes and the confining walls [47]. More specifically, chlorine substantially increases the total thermal conductivity within a specific temperature range, typically between 2000 K and 5000 K [45, 47]. At these intermediate temperatures, molecular chlorine (Cl_2) attacks almost all metals used in electrical contacts (copper. tungsten. silver) whilst simultaneously degrading solid insulators [47].

Likewise, the presence of hydrogen chloride or chlorine (HC, Cl_2) leads. in almost all cases. to accelerated corrosion [48]. This process results from the formation of volatile metal chlorides through reactions between the base metal. previously formed oxides. and aggressive gaseous compounds [48, 49]. By analogy with high-temperature industrial environments (furnaces. incinerators. and gasification plants). this mechanism also applies to Low Voltage circuit breakers subjected to atmospheres laden with HCl or Cl_2, particularly in the vicinity of the electric arc where metallic vapours resulting from contact erosion are present [48, 49]. Furthermore, a critical thermodynamic effect occurs: hydrogen chloride raises the dew point of the surrounding gas [50]. This aspect is especially significant for circuit breakers, as an elevated dew point means that moisture will condense at higher temperatures than expected in the presence of HCl. This moisture, combined with the chlorinated compounds, subsequently forms liquid hydrochloric acid, inducing massive electrochemical corrosion that compounds the high-temperature corrosion driven by the arc plasma [50, 51].

The general framework governing the corrosion, oxidation, and erosion mechanisms of silver-based contact materials used in low-voltage circuit breakers is now well established [52]. More specifically, when electrical contacts made of Ag, Ag/Ni, or Ag/MgO/NiO are exposed to an environment simultaneously containing SO_2, H_2S, NO_2, and Cl_2 under high temperature and high humidity conditions, a rapid increase in contact resistance is observed. This phenomenon is caused by the formation of a corrosion film composed primarily of silver chlorides and silver sulphides. SO_2 reacts with metallic surfaces (Cu, Ag) either via direct oxidation of the metal into copper sulphate $CuSO_4$ (a non-conducting compound) or, in the presence of moisture, through the formation of H_2SO_3 followed by H_2SO_4, which induce acidic electrochemical corrosion [48]. Experimental measurements conducted specifically on circuit breaker terminals have also demonstrated that contact resistance increases significantly with both SO_2 concentration and exposure duration, thereby degrading the electrical performance of the device [53]. Furthermore, recent studies combining calculations and endurance tests (20,000 operations) on Ag/SnO_2 composite materials commonly used in low-voltage applications have demonstrated that metal doping of the SnO_2 phase alters the Ag/SnO_2 wettability and reduces cathode-to-anode transfer, thereby limiting the formation of oxidized deposits responsible for contact resistance drift [54]. Within the arc plasma, the SO radical constitutes a reactive intermediate species that contributes to the reactive thermal conductivity, exhibiting a dissociation peak between 2500 K and 4000 K. It undergoes recombination at the cold periphery to reform SO2 and H_2SO_4 upon contact with the walls [45]. Consequently, SO_2 and its derivatives (H_2SO_3, H_2SO_4) also attack the epoxy resins and polyamides of the circuit breaker housings, causing their hydrolysis and reducing the dielectric strength of the arc chute walls [48, 49].

Nitrogen oxides, for their part act via synergistic mechanisms with the other species. The exposure of copper and silver to a combination of H_2S and NO_2 thus yields a corrosion rate up to five times higher than initially expected on silver [55]. Although the underlying mechanisms are not yet fully elucidated, the presence of NO_2 also accelerates the formation of silver sulphide (Ag_2S) [56]. In the presence of moisture, NO_2 forms nitrous acid (HNO_2) followed by nitric acid (HNO_3). The latter stands out as one of the most corrosive atmospheric pollutants: its high sticking coefficient on metallic surfaces confers a corrosive power on copper. zinc. and steel that is significantly superior to that of SO_2, NO_2, or O_3 under similar conditions [57]. Consequently, corrosion failures due to the condensation of gases containing H_2O, SO_3, NO_x, and HCl frequently occur in industrial plants, manifesting as general corrosion, pitting. and stress corrosion cracking [50]. Finally, HNO_3 attacks the glass-fibre-reinforced polymers constituting the housings and insulating walls of Low Voltage circuit breakers, inducing stress corrosion cracking.

5. Conclusions

In conclusion. this study demonstrates that the introduction of impurities such as H_2S, Cl_2, and SO_2 within the circuit breaker is highly detrimental to its operation, owing to a profound alteration of its equilibrium composition.

Compositional analysis reveals that the low-voltage circuit breaker is subjected to a synergy of chemical attacks that simultaneously compromise its three fundamental functions, namely steady-state conduction, arc interruption. and dielectric insulation. Primarily, the presence of sulphur and chlorine directly alters the transport properties of the plasma because the early ionisation of certain species significantly increases the electron density and, consequently. the electrical conductivity at low temperatures. This phenomenon extends the duration of the conducting phase and renders arc extinction more difficult. Furthermore, although the dissociation peaks of SO_2, SO, HCl, and Cl contribute to the reactive thermal conductivity, this effect remains ambivalent, whilst it promotes the radial thermal cooling of the plasma, it also maintains actively conducting zones at temperatures below the typical extinction threshold.

At the cold periphery, the recombined species (HCl, SO_2, NO_2, H_2SO_4, HNO_3) condense onto the electrodes. splitter plates. and insulating walls. This condensation simultaneously triggers high-temperature corrosion, via the formation of volatile metal chlorides and sulphates, and electrochemical corrosion induced by acidic solutions. The accumulation of resistive corrosion products (Ag_2S, $CuSO_4$, AgCl, and

$CuCl_2$) on copper. Silver, or tungsten contacts leads to a drastic rise in contact resistance. This generates excessive thermal heating which can ultimately result in device failure through contact welding or thermal runaway. This degradation exacerbates the intrinsic arc-induced erosion of the contacts. Recent energy balance assessments demonstrate that a significant fraction of the arc energy is transferred to the electrode and correlates directly with mass loss, thereby accelerating the overall failure kinetics in the presence of pollutants [58]. Beyond arc-related phenomena alone, in-service vibrations and repeated micro-displacements between contacts generate fretting phenomena. The coupled mechanisms of this process (wear, oxidation, and tribochemical corrosion) have been recently reviewed and are found to be strongly amplified by the presence of gaseous pollutants [59]. A recent quantitative model, coupling Joule heating, fretting amplitude, and surface corrosion, now enables the prediction of contact resistance drift in coated copper alloys, thereby paving the way for estimating the remaining useful life of circuit breakers exposed to the identified pollutants [60]. Finally. the combined action of HNO_3, H_2SO_4, and HCl causes the hydrolysis of the polymer matrices, reducing the dielectric strength of the arc chute walls and initiating stress corrosion cracking phenomena. This cumulative pressure on conventional materials (Ag, Ag-Ni, $AgSnO_2$) motivates the exploration of composite alternatives, such as Ag-Cu clad strips. However, recent studies demonstrate that these alternatives exhibit their own failure mechanisms via corrosion at the Ag-Cu interface, which must be taken into account in any comparative evaluation.

As a future prospect, this study will be extended to the calculation of thermodynamic properties and transport coefficients in order to precisely quantify the impact of H_2S, Cl_2, and SO_2 impurities on the arc interruption capability.

Abbreviations

LTE	Local Thermodynamic Equilibrium
NIST	National Institute of Standards and Technology

Acknowledgments

We used AI for translation and correction.

Author Contributions

Yaguibou Wepari Charles: Conceptualization, Data curation, Formal Analysis, Investigation, Methodology, Resources, Writing – original draft, Writing – review & editing

Beogo Cedric: Formal Analysis, Investigation, Methodology, Project administration, Resources, Software, Supervision, Validation

Korbeogo Aly Rachid: Investigation, Methodology, Project administration, Resources, Software, Supervision, Validation

Pafadnam Ibrahim: Investigation, Project administration, Resources, Software, Supervision, Validation

Banouga Adjigkiga: Software, Supervision, Validation, Visualization

Koalaga Zacharie: Resources, Software, Supervision, Validation, Visualization

Data Availability Statement

1) The data is available from the corresponding author upon reasonable request.
2) The data supporting the outcome of this research work has been reported in this manuscript:

Powars C. A. and Kendall R. M. in User's Manual. Aerotherm Chemical Equilibrium (A. C. E.) Computer Program. Aerotherm Corporation. Mountain View. California (1969).

J. Bacri and S. Raffanel. Calculation of Some Thermodynamic Properties of Air Plasmas: Internal Partition Functions. Plasma Composition. and Thermodynamic Functions. Plasma Chemistry and Plasma Processing. Vol. 7. No. 1. 1987.

Conflicts of Interest

The authors declare no conflicts of interest.

References

[1] Robert Morel. Low-voltage circuit breaker switching techniques, Technical Notebook 154, June 2000 edition, http://www.schneider-electric.com

[2] Andre, P., Courty, M.-A., Kagoné, A. K., Koalaga, Z., Kohio, N., Zougmore, F. Calculation of the chemical composition in a plasma produced from mixtures of PTFE, air, copper, and water vapor in the context of air-based electrical switching devices, International Journal of Technology, Innovation, Physics, Energy, and the Environment, 2016. vol. 2. no 1.

[3] Maintenance Guide for Masterpact NT and NW Circuit Breakers. Schneider Electric. 2021. LVPED508016FR-03. https://www.productinfo.schneider-electric.com

[4] Wepari, C. Y., Aly R K., Ibrahim P., Niessan K., Karim K., and Zacharie K. Calculation and Analysis of the Thermodynamic Properties of Air-Aerosols Mixtures, Advances in Materials Physics and Chemistry. 2025, 15(5). 75-89. https://doi.org/10.4236/ampc.2025.155005

[5] Yaguibou W C., Korsaga E., Kagone A., Kohio N., Koalaga Z., Zougmore F., Transport coefficients of air plasmas in an electrical circuit breaker. Journal of Physics of the SOAPHYS. 2019. Volume 1. pp. C19A11-1 à C19A11-5. https://doi.org/10.46411/jpsoaphys.19.01.011

[6] Wepari C Y., Niessan K., Abdoul K. K., and Zacharie K. Impact of Aerosol on Transport Coefficients of Air Thermal Plasmas in Circuit Breakers. International Journal of Engineering Research. 2018. Volume 7. Number 4. pp. 43-47. https://doi.org/10.5958/2319-6890.2018.00094.6

[7] Wepari C Y., Niessan K., Abdoul K K., Zacharie K., and François Z., Influence des aérosols sur la composition à l'équilibre d'un plasma d'air. Journal International de Technologie. de l'Innovation. de la Physique. de l'Energie et de l'Environnement. 2018. pp. 5-1 à 5-19.

[8] Yaguibou W. C., Korsaga E., Korbeogo A. R., Koalaga Z., and Zougmore F. Study of the composition of a plasma of dry air contaminated by Al_2O_3. CO. Fe_2O_3 and SiO_2. Advances in Materials Physics and Chemistry. 2022. Volume 12 Numéro 8. pp. 177- 193. https://doi.org/10.4236/ampc.2022.128013

[9] Cressault. Y., Hannachi. R., Teulet. P., Gleizes. A., Gonnet. J. and Battandier. J. Influence of Metallic Vapours on the Properties of Air Thermal Plasmas. Plasma Sources Science and Technology. 2008. 17. Article ID: 035016. https://doi.org/10.1088/0963-0252/17/3/035016

[10] Cressault. Y., Murphy. A. B., Teulet. P., Gleizes. A., and Schnick. M. Thermal Plasma Properties for Ar-Cu. Ar-Fe and Ar-Al Mixtures Used in Welding Plasmas Processes: II. Transport Coefficients at Atmospheric Pressure. Journal of Physics D: Applied Physics. 2013. 46. Article ID: 415207. https://doi.org/10.1088/0022-3727/46/41/415207

[11] Cressault. Y., Kimpeler. S., Moser A, and Teulet. P. Thermophysical Properties of Air-Pa66-Copper Plasmas for Low-Voltage Direct Current Switches. Plasma Physics and Technology. 2023. 10. pp 52-55. https://doi.org/10.14311/ppt.2023.1.52

[12] Adjigkiga B., Wepari C. Y., Abdoul K. K, Ibrahim P., Niéssan K., Zacharie K., and François Z. Determination of the Transport Coefficients of an Air Plasma Contaminated by $AgSnO_2$ Alloy Vapour. Journal of Physical Science. 2025. Vol. 36(2). 1-18. https://doi.org/10.21315/jps2025.36.2.1

[13] Banouga A., Kagoné A. K., Yaguibou W. C., Kohio N., Koalaga Z., Zougmoré F. Equilibrium Composition of a Plasma in the Low Voltage Air Circuit Breaker Contaminated by the Vapor of $AgSnO_2$ Alloy Electrical Contacts. Advances in Materials Physics and Chemistry. 2022. 12. 69-81. https://doi.org/10.4236/ampc.2022.125006

[14] Adjigkiga B., Abdoul K. K., Wepari C. Y., Niessan K., Zacharie K., and François Z. Determination of the thermodynamic properties of an air plasma contaminated by $AgSnO_2$ alloy vapor, Canadian Science Publishing. 2024. 00: 1-10. dx. https://doi.org/10.1139/cjp-2023-0052

[15] Kagone A. K., Kohio N., Yaguibou W. C., Koalaga Z., and Zougmore F. Transport Coefficients of Air - PMMA Mixtures Thermal Plasmas. American Journal of Materials Science and Engineering. 2020. Volume 8. n° 1. pp. 22-28. https://doi.org/10.12691/ajmse-8-1-4

[16] Kagone A. K., Kohio N., Yaguibou W. C., Koalaga Z., and Zougmore F. Calculation of the Chemical Composition of Air - PMMA Mixtures Thermal Plasmas, American Journal of Physical Chemistry. 2020, Volume 9. n° 2. pp. 27- 35. https://doi.org/10.11648/j.ajpc.20200902.12

[17] Kohio N., Kagone A. K., Yaguibou W. C., Koalaga Z., Zougmore F. Water Vapor Influence on Thermodynamic Properties of Air-water Vapor Mixtures Plasmas at Low Temperatures, International Journal of Physics. 2019, Volume 7 n° 3. pp. 66 - 72. https://doi.org/10.12691/ijp-7-3-1

[18] Kagone A. K., Kohio N., Yaguibou W C., Koalaga Z., and Zougmoré F. Thermodynamic properties calculation of air - water vapor mixtures thermal plasmas, Global Journal of Pure and Applied Sciences. 2018, Voume 24. n° 1. pp. 37 - 49. https://dx.doi.org/10.4314/gjpas.v24i1.5

[19] Kagone A K., Kohio N., Yaguibou W C., Koalaga Z., and Zougmoré F. Water Vapor Influence on Thermodynamic Properties of Air-water Vapor Mixtures Plasmas at Low Temperatures, International Journal of Physics. 2019, Volume 7. n° 3. 66 - 72. https://doi.org/10.12691/ijp-7-3-1

[20] Kagone A K., Kohio N., Yaguibou W. C., Koalaga Z., and Zougmoré F. Influence of Metallic Copper Vapors on the Chemical Composition of a Mixture of Air and Water Vapor Thermal Plasmas in the Temperature Range 1000 K to 20000K, American Journal of Nano Research and Applications. 2020, Volume 8. n° 3. 50-57. https://doi.org/10.11648/j.nano.20200803.13

[21] Li, X., Liu, L., Wang, W., Geng, Z., Analysis of Breaking Characteristics of C_4F_7N/CO_2 Mixture Gas in Circuit Breaker. Energies, 2024, 17(11), 2638. https://doi.org/10.3390/en17112638

[22] Wang, W., Yan, X., Wang, H., Gao, K. Comparative Studies of C_4F_7N-Based Gas Mixtures as the Eco-Friendly Alternative to SF_6 for Interrupting Applications. High Voltage, 2025, 10: 228-242. https://doi.org/10.1049/hve2.70003

[23] Hu, S., Qiu, R., Zhou, W. Dielectric Properties and Synergistic Effect Evaluation Method of C_4F_7N Mixtures. IEEE Transactions on Dielectrics and Electrical Insulation, 2024, 31, 793-800, https://doi.org/10.1109/TDEI.2023.3316632

[24] Liu, T., Ding, Y., Zhang, C., Kang, X. The Decomposition Mechanism of C_4F_7N-Ag Gas Mixture Under High Temperature Arc. Applied Sciences, 2026, 16(1), 356. https://doi.org/10.3390/app16010356

[25] Zhou, Y., Humphries, J. E., Spencer, J. W., Joseph D. Y., Wang Z, and Jones G. R. Contact Erosion Induced by Free-Burning Arcs in an Experimental Gas Circuit Breaker. IEEE Transactions on Power Delivery, 2025, https://doi.org/10.1109/TPWRD.2025.3543855

[26] Charles. Y. W., Moumouni. D., Nebon. B., Moumouni. S., Ibrahim. P., Karim. K. A., Zacharie. K. A study of the thermodynamic Characteristics of Air-Cl_2-H_2S Plasma in an Air Circuit Breaker. Current Journal of Applied Science and Technology. 2026. 45(5). 33-45. https://doi.org/10.9734/cjast/2026/v45i54692

[27] Godin D., and Trépanier J. Y. A robust and efficient method for the computation of equilibrium composition in gaseous mixtures. Plasma Chemistry and plasma processing. 2004. Vol 24. No 3.

[28] Boulos M I., Fauchais P., Pfender E. Thermal Plasmas: Fundamentals and Applications. 1994. Vol. 1. Plenum Press. New York. USA.

[29] Capitelli M., Colonna G., D'Angola A. Fundamental Aspects of Plasma Chemical Physics: Thermodynamics. Springer Series on Atomic. Optical. and Plasma Physics. 2012. Vol. 66. Springer. New York. USA.

[30] McBride B. J., Michael J. Z and Gordon. S. Thermodynamic Properties of Individual Species. Nasa Glenn Coefficients for Calculating. 2002. Glenn Research Center. 297.

[31] NIST Chemistry WebBook. Dissociation energies and ionization potentials. https://webbook.nist.gov

[32] Bendjebbar F., André P., Benbakkar M., Rochette D., Flazi S and Vacher D. Plasma Formed in Argon. Acid Nitric and Water Used in Industrial ICP Torches. Plasma Science and Technology. 2012. Vol. 14. No. 8. https://doi.org/10.1088/1009-0630/14/8/01

[33] Andre. P., Study of the composition and thermodynamic properties of thermal plasmas in and out of thermodynamic equilibrium. Ph.D. Thesis. Université Blaise Pascal de Clermont-Ferrand II (France). 1995.

[34] Cayet S. and Dudeck M. Chemical Equilibrium in Gaseous Mixtures under Thermal Non-Equilibrium, Journal de Physique III. EDP Sciences. 1996. 6 (3). pp. 403420. https://doi.org/10.1051/jp3:1996130

[35] P. Koukkari et R. Pajarre. A Gibbs energy minimization method for constrained and partial equilibria. Pure Appl. Chem. 2011. Vol. 83. No. 6. pp. 1243-1254. https://doi.org/10.1351/PAC-CON-10-09-36

[36] Rochette. D., Bussière W., and André P. Composition enthalpy. and Vaporisation temperature calculation of Ag-SiO_2 plasma with air in the temperature range from 1000 K to 6000K and for pressure included between 1- 50 bars, Plasma chemistry and plasma processing. 2004, Volume 24, pages 475-492.

[37] Powars C. A. and Kendall R. M. in User's Manual. Aerotherm Chemical Equilibrium (A. C. E.) Computer Program. Aerotherm Corporation. Mountain View. California (1969).

[38] J. Bacri and S. Raffanel. Calculation of Some Thermodynamic Properties of Air Plasmas: Internal Partition Functions. Plasma Composition. and Thermodynamic Functions, Plasma Chemistry and Plasma Processing. 1987, Vol. 7. No. 1.

[39] Wei J. L., Hao J., Bing T. L., Zi Y. C., Liang Z., Shu Y. J., Hai P. W., Wen Z. S. Metallic electrical contact materials: DFT calculations, wetting mechanism and arc resistance, Materials Today Physics, 2024, vol. 40, art. 101333, https://doi.org/10.1016/j.mtphys.2024.101333

[40] Christian F., Michel B., Pierre C., and Pascale P. Experimental and Numerical Studies of Arc Restrikes in Low-Voltage Circuit Breakers, IEEE transactions on plasma science. 1997, vol. 25, no. 5.

[41] P. Freton et J.-J. Gonzalez. Overview of current research into low-voltage circuit breakers, The Open Plasma Physics Journal. 2009, vol. 2. pp. 105-119.

[42] Boulos. M. I., Fauchais P. L, and Pfender E. Handbook of Thermal Plasmas. Springer. Cham. 2023. https://doi.org/10.1007/978-3-319-12183-3

[43] J. P. Trelles. C. Chazelas. A. Vardelle et J. V. R. Heberlein. "Arc Plasma Torch Modeling." Journal of Thermal Spray Technology. vol. 18. n° 5-6. pp. 728-752. 2009, https://doi.org/10.1007/s11666-009-9342-1

[44] Kopainsky. J. Influence of the Arc on Breakdown Phenomena in Circuit Breakers." in K. Ragaller (éd.). Current Interruption in High-Voltage Networks. Springer Science+Business Media New York. 1978.

[45] Murphy A. B. Transport coefficients of air. argon-air. nitrogen-air. and oxygen-air plasmas, Plasma Chemistry and Plasma Processing. 1995, vol. 15. n° 2. pp. 279-307, https://doi.org/10.1007/BF01459700

[46] Capitelli. M., Colonna. G., Gorse. C.; and D'Angola. A. Transport properties of high temperature air in local thermodynamic equilibrium, The European Physical Journal D. 2000, vol. 11. pp. 279-289, https://doi.org/10.1007/s100530070094

[47] Hannachi. R., Cressault. Y., Teulet. Ph., Ben Lakhdar Z., and Gleizes. A. Net emission of H_2O-air-$MgCl_2$/$CaCl_2$/NaCl thermal plasmas, Journal of Physics D: Applied Physics. 2008, vol. 41, art. 205212, https://doi.org/10.1088/0022-3727/41/20/205212

[48] Haanappel. V. A. C., Fransen T., and Gellings. P. J. Chlorine-Induced High Temperature Corrosion: I. Metals and Alloys A Review, High Temperature Materials and Processes. 1992, vol. 10. n° 2. pp. 67-90, https://doi.org/10.1515/HTMP.1992.10.2.67

[49] Grabke. H. J., Reese E., and Spiegel. M. The effects of chlorides. hydrogen chloride. and sulfur dioxide in the oxidation of steels below deposits, Corrosion Science. 1995, vol. 37. n° 7. pp. 1023-1043, https://doi.org/10.1016/0010-938X(95)00011-8

[50] Huijbregts W. M. M and Leferink. R. G. I. Latest advances in the understanding of acid dewpoint corrosion: corrosion and stress corrosion cracking in combustion gas condensates, Anti-Corrosion Methods and Materials. 2004, vol. 51. n° 3. pp. 173-188, https://doi.org/10.1108/00035590410533129

[51] Nielsen. H. P., Frandsen. F. J., Dam-Johansen K., and Baxter. L. L. The implications of chlorine-associated corrosion on the operation of biomass-fired boilers, Progress in Energy and Combustion Science. 2000, vol. 26. n° 3. pp. 283-298. https://doi.org/10.1016/S0360-1285(00)00003-4

[52] Kesim M. T., Yu H., Sun Y., Aindow M., Alpay S. P. Corrosion, Oxidation, Erosion and Performance of Ag/W-based Circuit Breaker Contacts: A Review, Corrosion Science, vol. 135, p. 12-34, 2018. https://doi.org/10.1016/j.corsci.2018.02.010

[53] Lu Jianguo, Wang Jingqin, Wang Lili, Liu Lin, Guan Ruiliang, Yu Xiaofeng, Zhao Sheng. Study on electrical contact performance of circuit breaker terminals in the environment containing SO_2, 26th International Conference on Electrical Contacts (ICEC 2012). IET. 2012, https://doi.org/10.1049/cp.2012.0621

[54] Wang H., Cai Q., Wang J., Zhang Y., Hu D., Wang Y. First-principles and experimental investigations on physical properties and arc erosion behavior of metal-doped $AgSnO_2$ electrical contact material, Ceramics International, 2023, vol. 49, p. 26033-26048, https://doi.org/10.1016/j.ceramint.2023.05.1054

[55] Chudnovsky. B. H. Degradation of power contacts in industrial atmosphere: silver corrosion and whiskers, Proceedings of the 48th IEEE Holm Conference on Electrical Contacts. Orlando. 2002, pp. 140-147. https://doi.org/10.1109/HOLM.2002.1040834

[56] M. Myers. Overview of the use of silver in connector applications, Advanced Plating Technologies Technical Paper. 2013, 503-1016, rev. O, 5feb09.

[57] Farid Samie., Johan Tidblad., Vladimir Kucera., Christofer Leygraf., Atmospheric corrosion effects of HNO_3 — comparison of laboratory-exposed copper. zinc and carbon steel, Atmospheric Environment. 2007, vol. 41(23): 4888-4896. https://doi.org/10.1016/j.atmosenv.2007.02.007

[58] Zhou Y., Humphries J., Spencer J., Yan J., Wang Z., Jones G. Contact erosion at high currents in high-voltage gas circuit breakers — Part II: Assessment of energy balance of arc-electrode interaction, IEEE Transactions on Power Delivery, 2024. https://doi.org/10.1109/TPWRD.2024.3519952

[59] D. Wang, J. Xu, F. Wang, Zhao Y., Xiang Z., Ding H. A comprehensive review on the fretting wear of electrical contact interface, Friction, 2025, vol. 13, n° 8, art. 9441012, https://doi.org/10.26599/FRICT.2025.9441012

[60] Meng H., Wanbin R and Zhang C. A Degradation Model of Electrical Contact Performance for Copper Alloy Contacts with Tin Coatings Under Power Current-Carrying Fretting Conditions, Coatings 2024, 14, 1587. https://doi.org/10.3390/coatings14121587

Biography

Yaguibou Wepari Charles is a teacher at Thomas SANKARA University, Dori University Cente. He completed his PhD in Plasma Physics and Electric Arcs from Joseph KI-ZERBO University in 2018, and his Master of Applied Physics from the same institution in 2014. Dr. Yaguibou was promoted to the rank of Maître-Assistant (Assistant Professor) by CAMES in 2023.

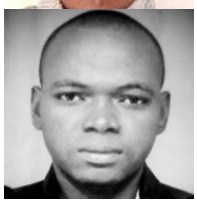

Beogo Cedric is a Research Scientist and an Assistant Professor of Physics at the Thomas SANKARA University (UTS). After completing a master's degree in applied physics in the field of nuclear science applications, he joined the national radiation protection and nuclear safety authority in 2014, where he carried out radiation source inspection activities in health centres and industries facilities. He was also in charge of drafting the procedures for samples analysing by gamma ray spectrometry and for radiological monitoring of the environment. In 2019, he defended his doctoral thesis on the measurement of natural radioactivity in two high background radioactivity areas of Burkina Faso. Then, he joined the university in 2020 where he currently teaches subjects such as Biophysics and Physics while carrying out research activities within the Laboratory of Materials and Environment (LAME) in the field of nuclear sciences within the radiation and matter team.

Korbeogo Aly Rachid is a lecturer and researcher in physics, specializing in materials mechanics. Since 2021, he has been based at the Polytechnic School of Ouagadougou in Burkina Faso, where he teaches physics. His research focuses primarily on numerical modeling in physics. He has worked on fracture mechanics under small deformations and the modeling of structures undergoing large deformations. Multiphysics and multifield environments have also captured his attention, particularly through his work on the numerical modeling of microstretch media and thermo-piezoelectric materials. He contributed to this work on the numerical aspect, specifically the management of the algorithm used to optimize the results.

Pafadnam Ibrahim is an assistant at the Science and Technology Training and Research Unit at Thomas SANKARA University in Ouagadougou. He obtained his PhD in applied physics in 2024 from Joseph KI-ZERBO University in Ouagadougou. He has participated in numerous international research projects in recent years. He has also participated in several international conferences on various topics. Dr. Ibrahim PAFADNAM is passionate about scientific research and innovation.

Banouga Adjigkiga earned his Master's degree in 2018 and recently defended his Ph.D. in 2024 at Joseph KI-ZERBO University. His research, conducted at the Laboratory of Materials and Environment, focused on plasma physics. His thesis work specifically investigated the impact of a silver-tin dioxide alloy ($AgSnO_2$) on the transport and thermodynamic properties of plasmas in circuit breakers. In addition to his research career, Mr. Banouga also works as a high school teacher.

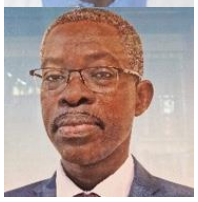

Koalaga Zacharie holds a Ph.D. in Electrotechnics from Université Blaise Pascal, France, earned in 1991. He is a distinguished Full Professor in Electronic, Electrotechnics, and Photovoltaic at the UFR-SEA Department of Physics. Currently, he serves as the Director of the Laboratory of Materials and Environment (LAME) at UJKZ, a position he has held since 2020. His extensive career includes significant leadership roles, such as serving as the President of the Scientific Council for both the ESUP-Jeunesse School and the IFIC-AUF in Tunis. He has also directed the open and distance learning institute at UJKZ and was the Academic Director of the ISGE-BF Institute. His research expertise lies in the physics of electrical arcs and plasmas, as well as photovoltaic systems. He actively coordinates research projects and conferences, including the RAMSES Network Center of Excellence and the ISAPA Symposium 2011. Additionally, he is a scientific editor for the Journal JITIPEE.

Research Field

Yaguibou Wepari Charles: Plasma Physics, Electric Arcs, Waste Management, Environment, Energy
Beogo Cedric: nuclear science, radiation protection
Korbeogo Aly Rachid: mechanics, numerical modelling
Pafadnam Ibrahim: Plasmas, Electric Arcs, Environment, Energy, Climat
Banouga Adjigkiga: Plasmas, Electric Arcs, Physics, Electric Arcs, Waste Management, Environment, Energy
Koalaga Zacharie: Electrical arc & Plasmas Physics, Photovoltaic systems